Journal of Solid State Chemistry **163,** 332–339 (2002)
doi:10.1006/jssc.2001.9427, available online at http://www.idealibrary.com on IDEAL®

# The Crystal Structures of the Binary Mixed Valence Compound $Bi_3^{(III)}Bi^{(V)}O_7$ and Isotypic $Bi_3SbO_7$ as Determined by High Resolution X-Ray and Neutron Powder Diffraction

Robert E. Dinnebier,* Richard M. Ibberson,† Helmut Ehrenberg,‡ and Martin Jansen*,[1]

*Max-Planck Institute for Solid State Research, Heisenbergstrasse 1, D-70569 Stuttgart, Germany; †ISIS Facility, CLRC—Rutherford Appleton Laboratory, Chilton, Didcot OX11 0QX, United Kingdom; and ‡TU Darmstadt, FB Material-und Geowissenschaften, Petersenstrasse 23, D-64287, Germany

Received July 31, 2001; in revised form October 2, 2001; accepted October 5, 2001

**The crystal structures of the mixed valence compound $Bi_3^{(III)}Bi^{(V)}O_7$ (1) and isotypic $Bi_3^{(III)}Sb^{(V)}O_7$ (2) were determined *ab initio* from powder diffraction data. At room temperature, both structures crystallize in space group $P\bar{1}$ ($Z = 2$) with $a = 6.7253(2)$, $b = 6.9950(2)$, $c = 7.7961(2)$ Å, $\alpha = 72.566(2)$, $\beta = 88.842(2)$, $\gamma = 76.925(2)^\circ$, and $V = 340.39(2)$ Å$^3$ for (1) and $a = 6.6044(3)$, $b = 7.0146(3)$, $c = 7.6048(3)$ Å, $\alpha = 73.388(2)$, $\beta = 89.225(2)$, $\gamma = 76.190(2)^\circ$, and $V = 327.28(2)$ Å$^3$ for (2). Combined Rietveld refinements based on both synchrotron and neutron powder patterns were performed ($T = 295$ K, $R$-Bragg = 5.4% for (1), $R$-Bragg = 6.4% for (2)). The crystal structures contain five crystallographically different anion polyhedra in two different coordination types and can be related to the $CaF_2$-type structure with the cations forming a distorted face centered cubic lattice and the oxygen atoms filling positions close to seven of the eight tetrahedral cavities.** © 2002 Elsevier Science

***Key Words:*** **high resolution X-ray powder diffraction; high resolution neutron powder diffraction; mixed valence compounds; bismuth oxide; fluorite structure type.**

## 1. INTRODUCTION

A number of years ago we provided conclusive evidence for $Bi_4O_7$ being a fully charge ordered pseudo-binary bismuth(III,V)oxide (1). This view had received significant support by the existence of an isostructural ternary phase $Bi_3^{(III)}Sb^{(V)}O_7$. Unfortunately, all attempts to grow single crystals of at least one of these compounds or to solve the crystal structure from powder diffraction data failed at that time.

Bismuth(III,V) mixed valency has attracted much attention since it seems to be the key for understanding superconductivity in $BaPb_{1-x}Bi_xO_3$ (2) and $Ba_{1-x}Bi_xO_3$ (3), which are the only copper-free oxidic high-temperature-superconductors (HTSC) known to date. The reports in the literature range from fully charged disordered species, as they can be found among the wide variety of bismuthdioxides (4), and the partially charge-ordered representatives $BaBiO_3$ (5) or $Ag_2BiO_3$ (6) to fully charge ordered systems like $Ag_{25}Bi_2{}^{(III)}Bi^{(V)}O_{18}$ (7) and $Bi^{(III)}Bi^{(V)}O_4$ (8). The latter, shown to be isostructural to $\beta$-$Sb_2O_4$ (9), has clearly distinct sites for the two valencies of bismuth, and thus it is most closely related to previously reported $Bi_4O_7$.

Since the powder diffraction techniques have been continuously developed to a powerful tool, (e.g., 10, 11) enabling the determination and refining of large and complex crystal structures *ab initio* (without using any preinformation), we felt encouraged to try again the structure determination of $Bi_4O_7$ using high resolution X-ray and neutron powder diffraction data.

## 2. EXPERIMENTAL

### 2.1. Materials and Methods

*2.1.1. Samples.* $Bi_3^{(III)}Bi^{(V)}O_7$ and $Bi_3SbO_7$ were synthesized using the procedure published previously (2).

*2.1.2. X-ray powder diffraction.* X-ray powder diffraction data were collected with the 3 circle Huber goniometer at the high resolution X-ray powder diffractometer at beamline B2 at the Hamburger Synchrotronstrahlungslabor (HASYLAB) (Fig. 1). The X-rays from the bending magnet source were collimated vertically by a Au-coated 1:1 focusing toroid at a distance of 18 m for (**1**) and by a Pt-coated cylindrical mirror at a distance of 17 m for (**2**) from the source before they are incident on a Ge(111) double crystal monochromator, which was used to select the X-ray energy of the experiment. The size of the beam was adjusted to approximately $2 \times 5$ mm$^2$ using slits. The wavelength was determined to be 1.24587(2) Å for (**1**) and 1.20649(2) Å for (**2**) from a silicon standard. The samples were contained in a flat plate sample holder big enough to avoid the

[1]To whom correspondence should be addressed. E-mail: martin@jansen.mpi-stuttgart.mpg.de.



0022-4596/02 $35.00

overspilling effect. The sample was rotated during measurements in order to improve randomization of the crystallites. The diffracted beam was analyzed with a Ge(111) crystal analyzer and detected with a Na(Tl)I scintillation counter. The incoming beam was monitored by another Na(Tl)I scintillation counter which measured the intensity from a scattering foil for normalization for the decay of the primary beam. In this parallel beam configuration, the resolution is determined by the analyzer crystal rather than by slits (12). Data were taken at room temperature in step scan mode for several hours and they were normalized against monitor counts. Experimental details for the different samples are given in Table 1. Low angle diffraction peaks had a FWHM of 0.031°2Θ for (**1**) and 0.023°2Θ for (**2**), still significantly broader than the resolution of the diffractometer which is estimated to be as low as 0.01°2Θ for the selected wavelength. Traces of an unknown second phase are visible in the scan of (**1**) but could clearly be distinguished from the main phase by their significantly broader peak shape. Data reduction was performed using the program GUFI (13).

Neutron powder diffraction patterns were collected at the high resolution powder diffractometer (HRPD) at the ISIS facility of the Rutherford Appleton Laboratory (RAL) (Fig. 1). The diffractometer is situated almost 100 m from the ISIS target at the end of a neutron guide with a resolution of $\Delta d/d \approx 4 \times 10^{-4}$ in the main backscattering detector bank which is effectively constant over the wide $d$-spacing range. The samples were contained in standard vanadium sample holders with 8 mm diameter and a filling height of 14 mm for (**1**) and 12 mm for (**2**). The time-of-flight (TOF) data were recorded in backscattering for 600 min for (**1**) and for 1000 min for (**2**) from 20 to 220 ms using fiber-optic-encoded ZnS scintillator detector modules which intersect the entire Debye–Scherrer rings over an angular range $160° \leq 2\Theta \leq 176°$. Data reduction was performed using the normalization and rebinning routines as described in the HRPD user's guide (14).

**TABLE 1**
**Crystallographic Data for $Bi_3^{(III)}Bi^{(V)}O_7$ and $Bi_3^{(III)}Sb^{(V)}O_7$**

| | $Bi_4O_7$ | $Bi_3SbO_7$ |
|---|---|---|
| Formula | $Bi_3^{(III)}Bi^{(V)}O_7$ | $Bi_3^{(III)}Sb^{(V)}O_7$ |
| Temperature [K] | 295 | 295 |
| Formula weight [g/mol] | 947.915 | 860.683 |
| Space group | $P\bar{1}$ | $P\bar{1}$ |
| $Z$ | 2 | 2 |
| $a$ [Å] | 6.7253(2) | 6.6044(3) |
| $b$ [Å] | 6.9950(2) | 7.0146(3) |
| $c$ [Å] | 7.7961(2) | 7.6048(3) |
| $\alpha$ [°] | 72.566(2) | 73.388(2) |
| $\beta$ [°] | 88.842(2) | 89.225(2) |
| $\gamma$ [°] | 76.925(2) | 76.190(2) |
| V [Å$^3$] | 340.39(2) | 327.28(2) |
| $\rho$-calc[g/cm$^3$] | 9.248 | 8.734 |
| TOF[ms], fixed angle [°2Θ] | 30–180, 168.33 | 20–180, 168.33 |
| 2Θ range [°],Step size [°2Θ] | 10.0–69.60, 0.006 | 5.5–64.5, 0.004 |
| Wavelength [Å] | 1.24587(2) | 1.20649(2) |
| $R$-p [%] (Sy, N) | 9.2, 11.3 | 15.1, 9.8 |
| $R$-wp [%] (Sy, N) | 11.6, 6.6 | 20.0, 9.0 |
| $R$-$F$ [%] (Sy, N) | 7.0, 10.0 | 5.9, 7.8 |
| $R$-$F^2$ [%](Sy, N) | 5.4, 16.5 | 6.4, 13.9 |
| No. of reflections (Sy/N) | 554, 2023 | 569, 2846 |

*Note.* $R$-p, $R$-wp, $R$-$F$, and $R$-$F^2$ refer to the Rietveld criteria (19) of fit for profile and weighted profile respectively, defined in (11). The Rietveld esd's for the lattice parameters have been multiplied by a factor of 4 according to (23).

### 2.2. Experimental Results

*2.2.1. X-ray powder diffraction.* Indexing with ITO (15) led to similar triclinic cells for **1** and **2**, with the possible space groups $P1$ or $P\bar{1}$ and two formula units in the unit cells. The peak profiles and precise lattice parameters were determined by LeBail-type fits (16) using the program Fullprof (J. R. Carvajal, personal communication). The background was modeled manually using GUFI (13). The peak-profile was described by a pseudo-Voigt function (17), in combination with a special function that accounts for the asymmetry due to axial divergence (18). The crystal structure of (**2**) was solved using the direct methods program EXPO (10). All cations and some candidates for the oxygen atoms could be found in default mode in space group $P\bar{1}$. Later refinements confirmed the correctness of this space group.

Rietveld refinements (19) for (**1**) and for the isostructural (**2**) were carried out in space groups $P\bar{1}$ and $P1$ using the GSAS program system (20). Lowering the space group symmetry to $P1$ resulted in only minor improvements of the fit, establishing $P\bar{1}$ as the correct space group. Rietveld refinements using the X-ray diffraction pattern were first carried out using the cations only. All oxygen atoms but one were then found in a cyclic way by difference-Fourier analysis followed by Rietveld refinements. The remaining oxygen atom was correctly guessed by chemical knowledge. A check on distances and angles revealed strong distortions from theoretical values due to the dominance of the strong scattering bismuth atoms in the electron density map. Finally, the simultaneous use of X-ray and neutron diffraction data in the Rietveld refinement, allowed the unconstrained refinement of all atomic positions and isotropic temperature factors in the crystal structures of (**1**) and (**2**). The Rietveld refinement converged quickly to the $R$-values given in Table 1. The positional parameters of the final Rietveld refinement and the isotropic temperature factors are presented in Table 2. The values for the anomalous dispersion corrections of the Bi and Sb atoms for the given wavelengths were taken from the KEK table (21) and have not been refined. It is noteworthy that the X-ray scattering

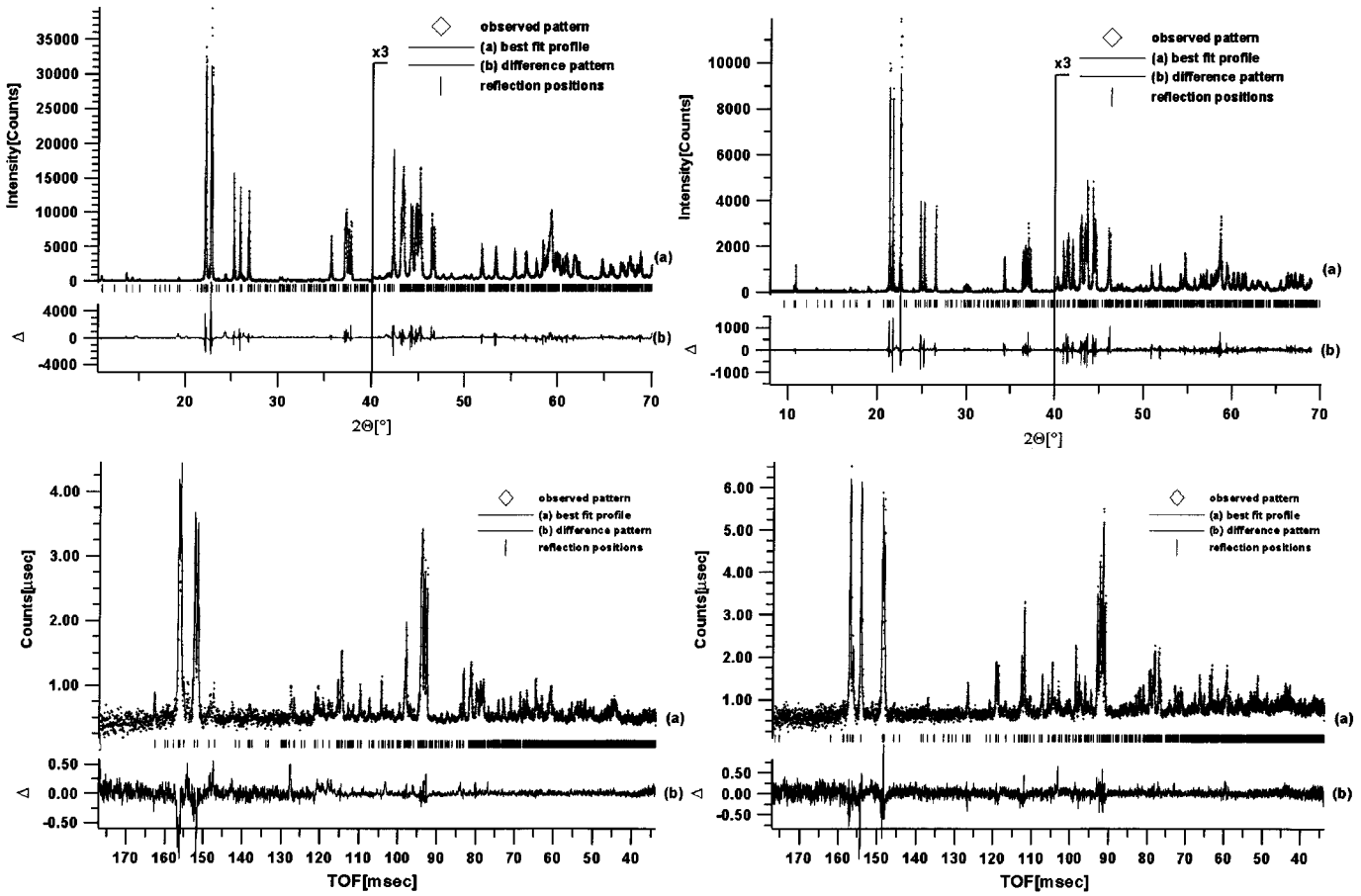


**FIG. 1.** Scattered X-ray (top) and neutron (bottom) intensity for (left) $Bi_3^{(III)}Bi^{(V)}O_7$ and (right) $Bi_3^{(III)}Sb^{(V)}O_7$ (right) at ambient conditions as a function of diffraction angle 2Θ and time of flight, respectively. Shown are the (diamonds) observed patterns, the (line) best Rietveld-fit profiles, and the difference curves between observed and calculated profiles in an additional window below. The high angle parts of the X-ray patterns are enlarged by a factor of 3, starting at 40° 2Θ.

**TABLE 2**
**Positional Parameters and $U_i/Å^2 \times 10^2$ for $Bi_3^{(III)}Bi^{(V)}O_7$ and $Bi_3^{(III)}Sb^{(V)}O_7$ at 295 K in $P\bar{1}$**

| | $Bi_4O_7$ | | | | $Bi_3SbO_7$ | | | |
|---|---|---|---|---|---|---|---|---|
| Atom | $x$ | $y$ | $z$ | $U_i$ | $x$ | $y$ | $z$ | $U_i$ |
| Bi(1) | 0.7293(4) | 0.4850(4) | 0.6253(4) | 1.3(1) | 0.7397(4) | 0.4612(4) | 0.6320(3) | 1.4(1) |
| Bi(2) | 0.2615(4) | 0.4930(5) | − 0.1213(4) | 1.0(1) | 0.2618(4) | 0.4980(5) | − 0.1240(3) | 1.3(1) |
| Sb/Bi(3) | 0 | 0 | 0 | 0.7(1) | 0 | 0 | 0 | 0.1(2) |
| Bi(4) | 0.4848(5) | 0.0042(5) | 0.2569(4) | 1.3(1) | 0.4899(5) | 0.0075(5) | 0.2543(4) | 1.3(1) |
| Sb/Bi(5) | 0 | 0 | $\frac{1}{2}$ | 1.0(1) | 0 | 0 | $\frac{1}{2}$ | 1.4(2) |
| O(1) | 0.108(2) | 0.684(2) | 0.040(2) | 1.3(3) | 0.120(2) | 0.704(2) | 0.036(1) | 1.4(3) |
| O(2) | 0.891(2) | 0.321(2) | 0.364(2) | 1.0(3) | 0.887(2) | 0.295(2) | 0.382(1) | 0.7(3) |
| O(3) | 1.105(2) | − 0.087(2) | 0.274(1) | 0.8(2) | 1.089(2) | − 0.065(2) | 0.269(1) | 0.8(2) |
| O(4) | 0.525(2) | 0.657(2) | 0.372(1) | 0.0(2) | 0.527(2) | 0.661(1) | 0.365(1) | 0.0(3) |
| O(5) | 0.287(2) | 0.070(2) | 0.521(2) | 1.7(3) | 0.271(2) | 0.052(2) | 0.524(1) | 1.4(3) |
| O(6) | 0.285(2) | 0.040(2) | − 0.057(2) | 1.4(3) | 0.274(2) | 0.047(2) | − 0.058(1) | 1.1(3) |
| O(7) | 0.472(2) | 0.365(2) | 0.195(1) | 0.8(3) | 0.469(2) | 0.374(2) | 0.187(1) | 0.9(3) |

power of Bi is almost three times higher than that of Sb which clearly allows to distinguish between these two cations with a synchrotron X-ray experiment without the need to use anomalous dispersion.

## 3. RESULTS AND DISCUSSION

### *3.1. Description of Crystal Structure*

The crystal structure of (**1**) and (**2**) contains two different types of cation polyhedra and five crystallographically different cation positions (Fig. 2; Table 3) forming the framework structure. The bismuth (respectively antimony) atoms located on inversion centers (Bi/Sb(3) at site 1*a* and Bi/Sb(5) at site 1*b*) are coordinated by oxygen atoms forming an almost regular octahedron with a mean distance of 2.08 Å for bismuth and 1.98 Å for antimony. Three bismuth atoms on general positions (Bi(1), Bi(2), and Bi(4)) are located in the apex of a distorted trigonal pyramid formed by oxygen atoms located at a distance of 2.08 to 2.28 Å and four more oxygen atoms located irregularly at distances of 2.40 to 3.02 Å. Regarding the differences of trivalent and pentavalent bismuth in terms of ionic radii, and the effect of the stereoactive $6s^2$ lone pair of $Bi^{(III)}$ (respectively, $5s^2$ for $Sb^{(III)}$), it is evident that the two special positions (1*a* and 1*b*) in the crystal structure of **1** and **2** are occupied by $Bi^{(V)}$, respectively $Sb^{(V)}$ cations, whereas the $Bi^{(III)}$ cations are located on the three general positions.

For clarity, the three-dimensional framework structure will be split in to two alternating sheets perpendicular to *b**-direction consisting of different kinds of coordination polyhedra (Fig. 3). The two differerent $Bi^{(V)}O_6$ (respectively, $Sb^{(V)}O_6$) octahedra share common vertices in trans-position thus forming infinite tilted chains along the *c* axis with the connecting oxygen atoms including an angle of 135.1°. $Bi(4)^{(III)}O_3$ trigonal pyramids are attached to the chains in an alternating fashion with two vertices of consecutive octahedra shared with two vertices of the trigonal base plane of the trigonal pyramid, and the bismuth atoms pointing up on one side of the chain and down on the other. Between the resulting parallel chains, no bonded contacts exist, thus leaving enough space for the stereoactive lone electron pair of the $Bi(4)^{(III)}$ atom. The second sheet consists of tetramers "$Bi_4^{(III)}O_8$" formed by 4 $Bi^{(III)}O_3$ trigonal pyramids in the following way: Two $Bi(1)^{(III)}O_3$ trigonal pyramids with the vertex in $\pm a$-direction share a common edge of their base planes thus forming a dimer (the crystallographic inversion

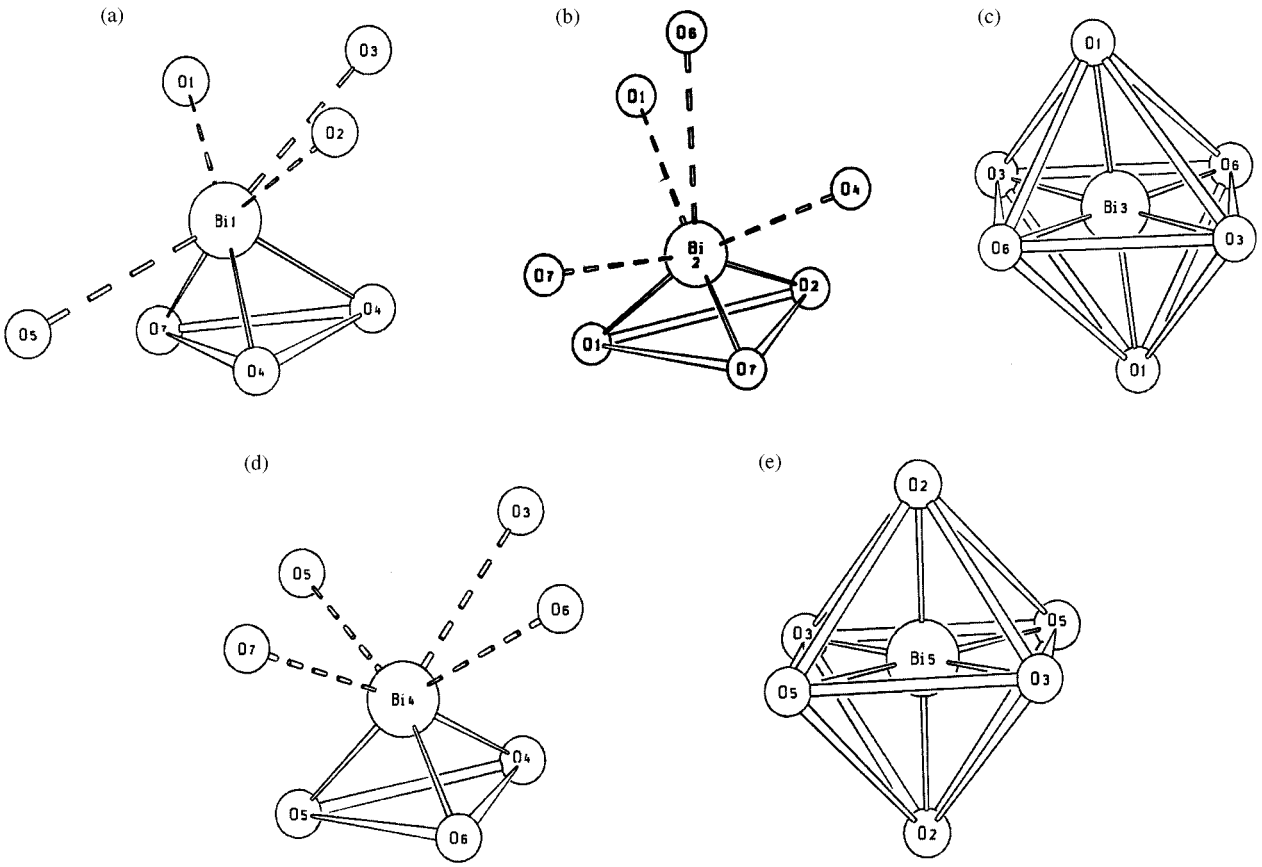


**FIG. 2.** The two types of the five crystallographically different cation polyhedra in the crystal structures of $Bi_3^{(III)}Bi^{(V)}O_7$ (respectively, $Bi_3^{(III)}Sb^{(V)}O_7$). (c), (e): regular $Bi^{(V)}O_6$ (respectively, $Sb^{(V)}O_6$) octahedra; (a), (b), (d): distorted $Bi^{(III)}O_{3+4}$ trigonal pyramids.

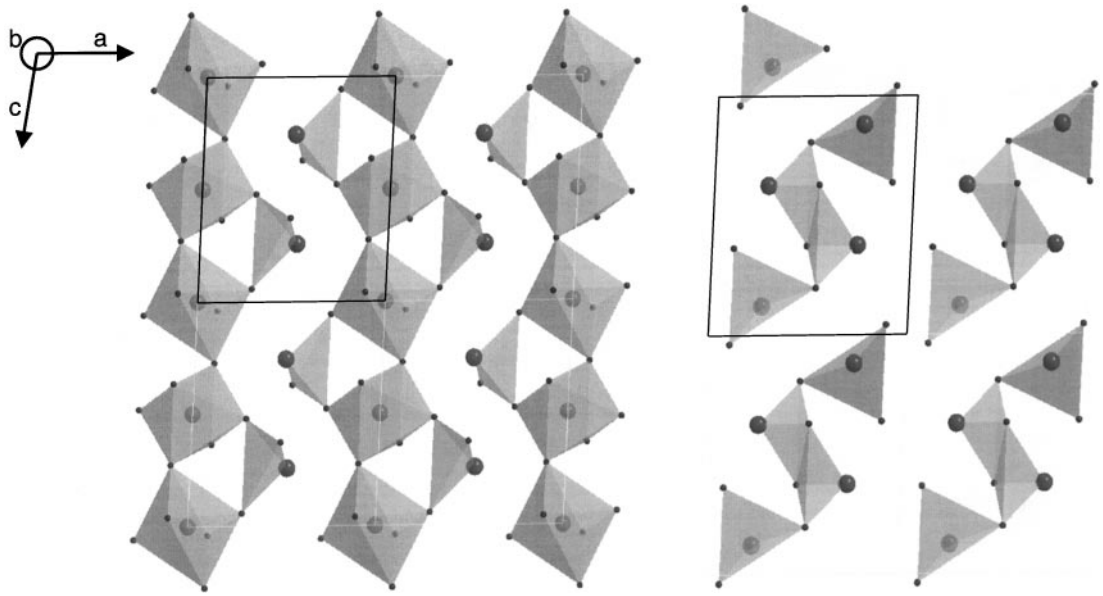


**FIG. 3.** For easier viewing the crystal structure of $Bi_3^{(III)}Bi^{(V)}O_7$ (respectively, $Bi_3^{(III)}Sb^{(V)}O_7$) is split in two "sheets" perpendicular to $b^*$-direction. The top sheet (left) consists of infinite tilted chains of $Bi^{(V)}O_6$ (respectively $Sb^{(V)}O_6$) octahedra along the $c$ axis and attached $Bi(4)^{(III)}O_3$ trigonal pyramid. The second layer (right) consists of "$Bi_4^{(III)}O_8$"-tetramers.

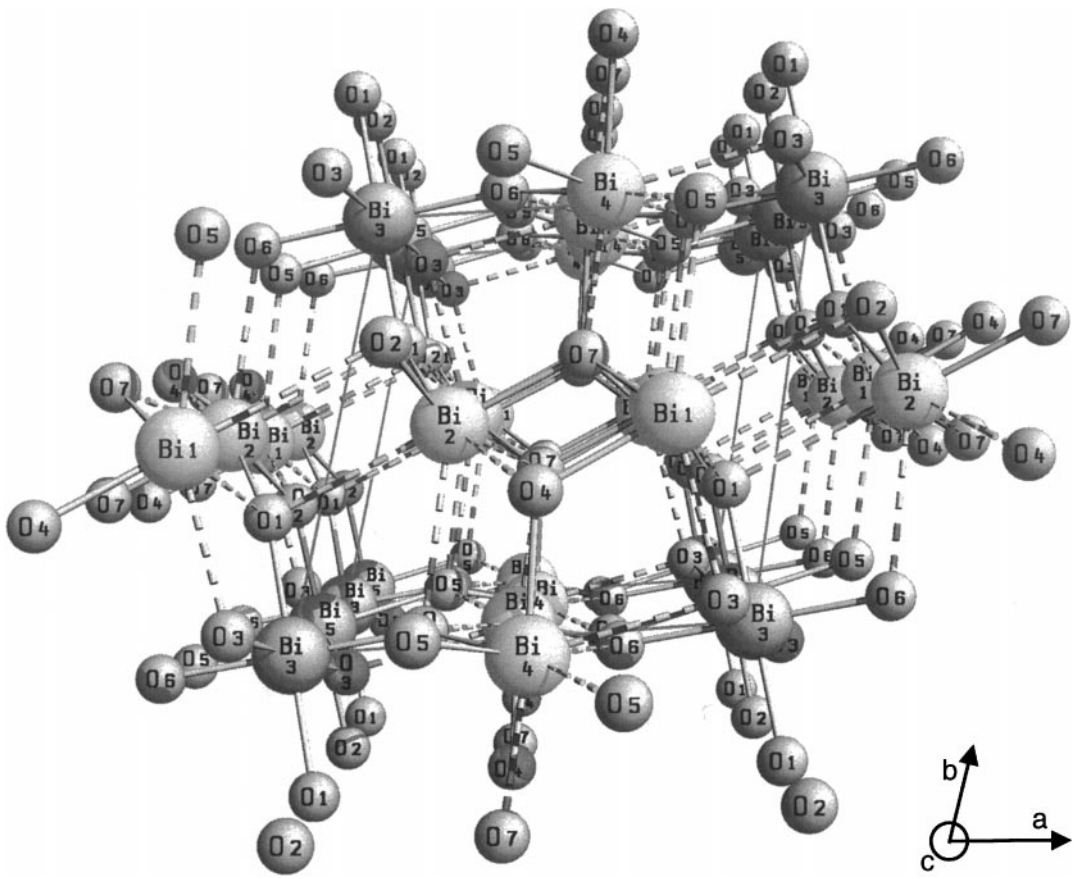


**FIG. 4.** Ball and stick representation of the crystal structure of $Bi_3^{(III)}Bi^{(V)}O_7$ (respectively, $Bi_3^{(III)}Sb^{(V)}O_7$) viewed down the $c$ axis. The chains of puckered $Bi^{(V)}O_6$- (respectively $Sb^{(V)}O_6$)-octahedra along the $c$ axis are clearly visible. Broken bonds indicate long bonds ( $> 2.4$ Å) between the bismuth and oxygen atoms.

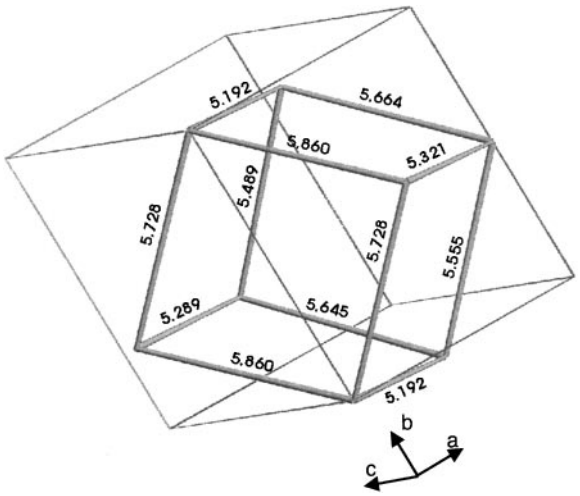


**FIG. 5.** The triclinic unit cell (thin lines) as well as the corresponding irregular *F*-centered *pseudo* (cubic) unit cell with an average unit cell length of 5.544 Å of $Bi_3^{(III)}Bi^{(V)}O_7$ (respectively, $Bi_3^{(III)}Sb^{(V)}O_7$) are shown. The $(\bar{2}10)$ plane of the triclinic unit cell corresponds to the closed packed (111) plane in the *pseudo*-fcc lattice.

**TABLE 3**
**Selected Distances and Angles for $Bi_3^{(III)}Bi^{(V)}O_7$ and $Bi_3^{(III)}Sb^{(V)}O_7$ at 295 K in $P\bar{1}$**

| Distances [Å] | $Bi_4O_7$ | $Bi_3SbO_7$ |
|---|---|---|
| Bi(1)–O(4) | 2.16(1) | 2.13(1) |
| Bi(1)–O(7) | 2.25(1) | 2.29(1) |
| Bi(1)–O(4′) | 2.27(1) | 2.36(1) |
| Bi(1)–O(1) | 2.66(1) | 2.54(1) |
| Bi(1)–O(2) | 2.72(1) | 2.57(1) |
| Bi(1)–O(3) | 2.63(1) | 2.63(1) |
| Bi(1)–O(5) | 2.96(1) | 3.26(1) |
| Bi(2)–O(2) | 2.08(1) | 2.16(1) |
| Bi(2)–O(1) | 2.18(1) | 2.18(1) |
| Bi(2)–O(7) | 2.23(1) | 2.17(1) |
| Bi(2)–O(7′) | 2.67(1) | 2.56(1) |
| Bi(2)–O(4) | 2.72(1) | 2.63(1) |
| Bi(2)–O(6) | 3.02(1) | 3.04(1) |
| Bi(2)–O(1′) | 3.00(1) | 3.15(1) |
| Sb/Bi(3)–O(1) | 2.09(1) 2*x* | 1.98(1) 2*x* |
| Sb/Bi(3)–O(6) | 2.02(1) 2*x* | 1.94(1) 2*x* |
| Sb/Bi(3)–O(3) | 2.12(1) 2*x* | 2.02(1) 2*x* |
| Bi(4)–O(5) | 2.20(1) | 2.21(1) |
| Bi(4)–O(6) | 2.21(1) | 2.19(1) |
| Bi(4)–O(4) | 2.28(1) | 2.29(1) |
| Bi(4)–O(7) | 2.40(1) | 2.44(1) |
| Bi(4)–O(5′) | 2.53(1) | 2.55(1) |
| Bi(4)–O(6′) | 2.74(1) | 2.70(1) |
| Bi(4)–O(3) | 2.76(1) | 2.81(1) |
| Sb/Bi(5)–O(3) | 2.09(1) 2*x* | 1.99(1) 2*x* |
| Sb/Bi(5)–O(2) | 2.14(1) 2*x* | 1.96(1) 2*x* |
| Sb/Bi(5)–O(5) | 2.12(1) 2*x* | 1.93(1) 2*x* |
| Bi(1)–Bi(1) (short) | 3.6216(4) | 3.616(4) |
| Bi(2)–Bi(1) (short) | 3.680(4) | 3.633(4) |
| O(4)–O(4) (short) | 2.56(1) | 2.68(1) |
| O(2)–O(3) (short) | 2.80(1) | 2.67(1) |
| O(1)–O(3) (short) | 2.76(2) | 2.69(2) |
| **Angles [°]** | **$Bi_4O_7$** | **$Bi_3SbO_7$** |
| O(6)–Sb/Bi(3)–O(1) | 89.3(5), 90.7(5) | 88.8(5), 91.2(5) |
| O(6)–Sb/Bi(3)–O(3) | 85.4(5), 94.6(5) | 87.7(4), 92.3(4) |
| O(1)–Sb/Bi(3)–O(3) | 81.8(4), 98.2(4) | 84.6(4), 95.4(4) |
| O(3)–Sb/Bi(5)–O(5) | 87.1(5), 92.9(5) | 92.4(4), 87.6(4) |
| O(3)–Sb/Bi(5)–O(2) | 83.0(5), 97.0(5) | 95.2(4), 84.9(4) |
| O(5)–Sb/Bi(5)–O(2) | 94.0(5), 86.0(5) | 90.9(5), 89.1(5) |
| O–Bi(1)–O | 56.4(3).. 125.5(4) | 61.8(3).. 128.3(3) |
| O–Bi(2)–O | 58.2(3)..127.2(4) | 71.6(4).. 110.8(3) |
| O–Bi(4)–O | 66.2(4).. 127.9(4) | 74.6(4).. 115.6(3) |

center is located in the middle of the common edge). The remaining corners of the two $Bi(1)^{(III)}O_3$ trigonal pyramids share a corner each with $Bi(2)^{(III)}O_3$ trigonal pyramids with their vertices in $\pm b$*-direction thus completing the tetramer. Again, this arrangement leaves enough space for the stereoactive electron pairs of the $Bi^{(III)}$ cations. The individual tetramers are not connected within the sheet. To complete the three-dimensional network, the two layers are linked by common corners (Fig. 4): The four yet unconnected corners of the tetramer belonging to $Bi(2)^{(III)}O_3$ trigonal pyramids are shared with corners of $Bi^{(V)}O_6$ (respectively, $Sb^{(V)}O_6$) octahedra above and below. In addition, the corners of the common edge of the two $Bi(1)^{(III)}O_3$ trigonal pyramids of the tetramer are shared with the remaining yet unconnected corners of the $Bi(4)^{(III)}O_3$ trigonal pyramids belonging to the sheets above and below.

The basic structural principle can be deduced from a projection of the $(\bar{2}10)$ plane of the triclinic unit cell of (**1**) or (**2**) which immediately reveals the pseudo-face-centered-cubic arrangement of the cations (Fig. 5). Indeed, a pseudo (cubic) unit cell with an average unit cell length of 5.544 Å (5.19–5.86 Å) and approximately 90° angles can be found with half the unit cell volume of the triclinic unit cell. It should be noted that the neighbor cells are similar but not identical to the reduced cell and that the $Bi^{(V)}$ and $Bi^{(III)}$ cations are treated as being equal. The structural relationship between this pseudo cell and the fluorite ($CaF_2$) structure type is evident (Fig. 6). In the fluorite structure, the cations form a face centered cubic (fcc) lattice with the anions sitting in the center of all 8 tetrahedral cavities and thus forming "$CaF_8$-cubes" as coordination polyhedra. $Bi_2O_4$ (8) which adopts a $\beta$-$Sb_2O_4$ type of structure, can be regarded as a distorted fluorite type of structure with all tetrahedral cavities filled by anions but shifted away from the center of gravity. The same holds for the title compound with the oxygen atoms filling positions close to seven of the eight tetrahedral cavities. In continuation of this structural principle two of the eight tetrahedral cavities are not occupied in the crystal structure of $\alpha$-$Mn_2O_3$ (Bixbyite). Further reduction of the number of anions in tetrahedral cavities

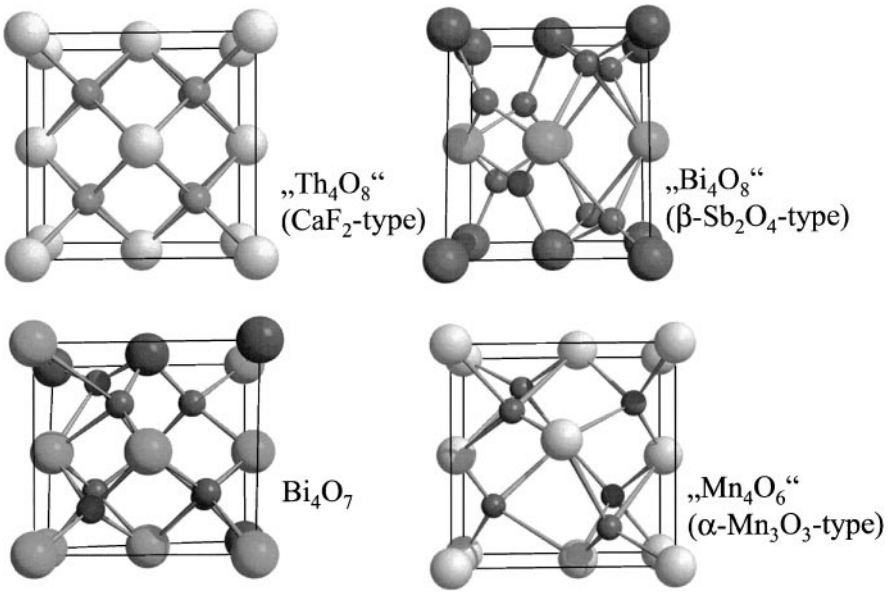


**FIG. 6.** Structural relationship between the (top left) ideal fluorite structure ($CaF_2$-type) and cut outs of the (top right) crystal structures of $Bi_2O_4$ ($\beta$-$Sb_2O_4$-type), (bottom left) $Bi_3^{(III)}Bi^{(V)}O_7$, and (bottom right) $\alpha$-$Mn_2O_3$ (Bixbyite) showing different distortions of the fcc lattice and a decreasing number of filled tetrahedral voids from eight down to six.

while keeping the fcc packing of the cations is realized in tetragonal $Bi_2O_{2.5}$ (22), which adopts a crystal structure similar to $\alpha$-$Mn_2O_3$ with one of its two crystallographically distinct oxygen atoms showing a fractional occupancy of 75%.

The examples of $Bi_4O_7$ along with $Bi_2O_4$ clearly show that pentavalent bismuth can exist in an oxidic environment as well as in the absence of stabilizing easily polarizable counter cations. Thus their existence suggests that crystalline $Bi_2O_5$ should also be accessible.

## 4. CONCLUSION

Using high resolution X-ray and neutron powder diffraction, it was possible to fully characterize the crystal structures of $Bi_3^{(III)}Bi^{(V)}O_7$ and isotypic $Bi_3^{(III)}Sb^{(V)}O_7$ at room temperature. The new structure type can be related to the fluorite structure and may be regarded as the missing link between $\beta$-$Sb_2O_4$ and $\alpha$-$Mn_2O_3$ structure types.

The complementary character of high-resolution X-ray- and neutron diffraction techniques applied to polycrystalline powder samples provides powerful combined constraints for the interpretation of experimental results. While X-ray diffraction is sensitive to the cation framework and clearly allows to distinguish between antimony and bismuth atoms, neutron diffraction enables the determination of the anion positions to high precision, thus allowing a detailed geometric interpretation of the crystal structure similar to what could be achieved had single crystals been available.

## ACKNOWLEDGMENTS

Financial support by the Deutsche Forschungsgemeinschaft (DFG) and the Fonds der chemischen Industrie (FCI) is gratefully acknowledged.

## REFERENCES

1. B. Begemann and M. Jansen, *J. Less-Common Metals* **156,** 123–135 (1989).
2. D. T. Marx, P. G. Radaelli, J. D. Jorgensen, R. L. Hitterman, D. G. Hinks, S. Pei, and B. Dabrowski, *Phys. Rev. B* **46**(2), 1144–1156 (1992).
3. R. J. Cava, B. Batlogg, J. J. Krajewski, R. J. Farrow, L. W. J. Rupp, A. E. White, K. T. Short, W. F. Peck, and T. V. Kometani, Nature **332**(6167), 814–816 (1988); H.-K. Fun, A. Wang, C.-H. Chou, T.-J. Lee, H.-Y. Tang, M. K. Wu, L.-S. Liou, and J.-C. Wang, *Chinese J. Phys. (Taipei)* **31**(6), 1157–1162 (1993).
4. “Gmelins Handbuch für anorganische Chemie, Bismut-Ergänzungsband, 8,” p. 642. Weinheim, 1964.
5. R. Arpe and Hk. Mueller-Buschbaum, *Z. Anorg. Allg. Chemie* **434,** 73–77 (1977).
6. S. Deibele and M. Jansen, *J. Solid State Chem.* **147,** 117–121 (1999).
7. M. Bortz and M. Jansen, *Angew. Chem.* **103**(7), 841–842 (1991), *Int. Ed. Engl.* **30**(7), 883–884 (1991).
8. N. Kumada, N. Kinomura, P. M. Woodward, and A. W. Sleight, *J. Solid State Chem.* **116,** 281–285 (1995).
9. J. Amador, E. Gutierrez-Puebla, M. A. Monge, I. Rasines, and C. Ruiz-Valero, *Inorg. Chem.* **27,** 1367–1370 (1988).
10. A. Altomare, M. C. Burla, M. Camalli, B. Carrozzini, G. L. Cascarano, C. Giacovazzo, A. Guagliardi, A. G. G. Moliterni, G. Polidori, and R. Rizzi, *J. Appl. Crystallogr.* **32,** 339–340. (1999).
11. J. I. Langford and D. Louër, *Rep. Prog. Phys.* **59,** 131–234 (1996).

12. D. E. Cox, *in* "Handbook of Synchrotron Radiation" (G. Brown and D. E. Moncton, Eds.), Vol. 3, Ch. 5 Powder Diffraction. Elsevier, Amsterdam, 1991.
13. R. E. Dinnebier and L. W. Finger, *Z. Krist. Suppl.* **15,** 148 (1998); available at http://www.pulverdiffraktometrie.de.
14. R. M. Ibberson, W. I. F. David, and K. S. Knight, "The High Resolution Neutron Powder Diffractometer (HRPD) at ISIS—A User Guide." Rutherford Appleton Laboratory Report RAL-92-031. (1992); available at http://www.isis.rl.ac.uk/crystallography/documentation/HRPDguide.htm#DATA COLLATION AND REDUCTION PROGRAMS)
15. J. W. Visser, *J. Appl. Crystallogr.* **2,** 89-95 (1969).
16. A. LeBail, H. Duroy, and J. L. Fourquet, *Mat. Res. Bull.* **23,** 447–452 (1988).
17. P. Thompson, D. E. Cox, and J. B. Hastings, *J. Appl. Crystallogr.* **20,** 79–83 (1987).
18. L. W. Finger, D. E. Cox, and A. P. Jephcoat, *J. Appl. Cryst.* **27,** 892–900 (1994).
19. H. M. Rietveld, *J. Appl. Crystallogr.* **2,** 65–71 (1969).
20. A. C. Larson and R. B. Von Dreele, "GSAS—General Structure Analysis System." Los Alamos National Laboratory Report LAUR 86-748 (1994); available by anonymous FTP from mist.lansce.lanl.gov.
21. S. Sasaki, S. KEK Report 88–14 (1989); Available at Technical Information & Library, National Laboratory for High Energy Physics, 1-1 Oho, Tsukuba-shi, Ibaraki-ken, 305, Japan, 136 pages.
22. A. A. Zav'yalova and R. M. Imamov, *Kristallografiya* **16,** 615–619 (1971).
23. J.-F. Bérar, "Accuracy in Powder Diffraction II," NIST Special Publication No. 846, pp. 63–67, 1992.